Prepared for submission to JCAP

CLASH-VLT: Testing the Nature of Gravity with Galaxy Cluster Mass Profiles

L. Pizzuti,[1] **B. Sartoris,**[1,2] **S. Borgani,**[1,2,3] **L. Amendola,**[4] **K. Umetsu,**[5] **A. Biviano,**[2] **M. Girardi,**[1,2] **P. Rosati,**[7] **I. Balestra,**[2] **G. B. Caminha,**[6] **B.Frye,**[11] **A. Koekemoer,**[10] **C. Grillo,**[8] **M. Lombardi,**[12] **A. Mercurio,**[9] **M. Nonino**[2]

[1]Dipartimento di Fisica, Sezione di Astronomia, Università di Trieste,
Via Tiepolo 11, I-34143 Trieste, Italy

[2]INAF - Osservatorio Astronomico di Trieste,
Via Tiepolo 11, I-34143 Trieste, Italy

[3]INFN - Sezione di Trieste,
Via Valerio 2, I-34127 Trieste, Italy

[4]Institut für Theoretische Physik, Universität Heidelberg,
Philosophenweg 16, D-69120 Heidelberg, Germany

[5]5 Institute of Astronomy and Astrophysics, Academia Sinica, P.O. Box 23-141,
Taipei 10617, Taiwan

[6]Dipartimento di Fisica e Scienze della Terra, Università di Ferrara,
Via Saragat 1, I-44122 Ferrara, Italy

[7]University Observatory Munich, Scheinerstrasse 1, D-81679 Muïchen, Germany

[8]Dark Cosmology Centre, Niels Bohr Institute, University of Copenhagen,
Juliane Maries Vej 30, DK-2100 Copenhagen, Denmark

[9]Osservatorio Astronomico di Capodimonte,
Via Moiariello 16, I-80131 Napoli, Italy

[10]Space Telescope Science Institute, 3700 San Martin Drive, Baltimore, MD 21208, USA

[11]Steward Observatory/Department of Astronomy, University of Arizona, 933 N Cherry Ave,
Tucson, AZ 85721, USA

[12]Dipartimento di Fisica, Università degli Studi di Milano, via Celoria 16, I-20133 Milan, Italy

E-mail: pizzuti@oats.inaf.it, barbara.sartoris@gmail.com, borgani@oats.inaf.it, l.amendola@thphys.uniheidelberg.de

Abstract. We use high-precision kinematic and lensing measurements of the total mass profile of the dynamically relaxed galaxy cluster MACS J1206.2-0847 at $z = 0.44$ to estimate the value of the ratio $\eta = \Psi/\Phi$ between the two scalar potentials in the linear perturbed Friedmann-Lemaitre-Robertson-Walker metric. An accurate measurement of this ratio, called anisotropic stress, could show possible, interesting deviations from the predictions of the theory of General Relativity, according to which Ψ should be equal to Φ. Complementary kinematic and lensing mass profiles were derived from exhaustive analyses using the data from the Cluster Lensing And Supernova survey with Hubble (CLASH) and the spectroscopic follow-up with the Very Large Telescope (CLASH-VLT). Whereas the kinematic mass profile tracks only the time-time part of the perturbed metric (i.e. only Φ), the lensing mass profile reflects the contribution of both time-time and space-space components (i.e. the sum $\Phi + \Psi$). We thus express η as a function of the mass profiles and perform our analysis over the radial range $0.5\,\mathrm{Mpc} \leq r \leq r_{200} = 1.96\,\mathrm{Mpc}$. Using a spherical Navarro-Frenk-White mass profile, which well fits the data, we obtain $\eta(r_{200}) = 1.01^{+0.31}_{-0.28}$ at the 68% C.L. We discuss the effect of assuming different functional forms for mass profiles and of the orbit anisotropy in the kinematic reconstruction. Interpreting this result within the well-studied $f(R)$ modified gravity model, the constraint on η translates into an upper bound to the interaction length (inverse of the scalaron mass) smaller than 2 Mpc. This tight constraint on the $f(R)$ interaction range is however substantially relaxed when systematic uncertainties in the analysis are considered. Our analysis highlights the potential of this method to detect deviations from general relativity, while calling for the need of further high-quality data on the total mass distribution of clusters and improved control on systematic effects.

Keywords: Galaxy clusters, modified gravity, gravitational lensing, dark energy theory, cosmology of theories beyond the SM

Contents

1 Introduction

In the current picture of cosmological studies, the standard ΛCDM model seems to be the most suitable to describe the expansion history, constrained with a wide range of observations (e.g. ref. [1]). In this scenario, the nature of Dark Energy, which is invoked to explain the current accelerating expansion (e.g. ref. [2]) and which should represent about 70% of the total density of the Universe, is still unknown. Several alternatives have been proposed to explain cosmic acceleration, including the possibility of introducing a modification of the Einstein's field theory of General Relativity (hereafter GR), assumed in the Standard Cosmological model. These models are expected not only to reproduce the expansion history, but also to match general relativity at scales comparable with those of the Solar System, where the theory is tested to high precision. Besides an accelerated expansion, a modification of GR should manifest itself also through its effect on the evolution of density perturbations. A possible evidence of modified gravity should also involve a change into the relation between the scalar potentials which appear in the perturbed Friedmann-Lemaitre-Robertson-Walker (hereafter FLRW) metric and the fluctuations in the matter density field (ref. [3]). Suitable parameterizations of these relations allow one to characterize deviations from GR as a function of redshift and scale (e.g. see ref. [4] and references therein).

In this paper we constrain deviations from GR by comparing mass profiles of galaxy clusters as derived from gravitational lensing and from a kinematic analysis of member galaxies. In fact, galaxies moving within clusters under the action of gravity only feel the time-time part of the perturbed FLRW metric, which is expressed by the potential Φ. On the other hand, the geodesics along which photons propagate within clusters reflect the contribution of both time-time and space-space components of the linear metric perturbations, i.e. they feel the sum of the two potentials $\Phi+\Psi$. Since $\Phi = \Psi$ in standard gravity with non-relativistic matter sources, mass profiles obtained from kinematic and lensing analyses, under the assumption of GR, should coincide as long as GR itself is valid. In other words, under the assumption that astrophysical and observational systematics are well understood for both the kinematic and lensing analyses, any deviation of mass profiles based on using either photons or galaxies as tracers of the metric perturbations should reflect a deviation from GR.

In the following, as a case study, we present results from MACS J1206.2-0847 (hereafter MACS 1206) a galaxy cluster at redshift $z = 0.44$ for which high-quality imaging and spectroscopic data have been analysed in detail as part of the Cluster Lensing And Supernova

survey with Hubble (CLASH, ref. [5]) and the spectroscopic follow-up with the Very Large Telescope (CLASH-VLT, ref. [6]) programs. By using the reconstructed mass density profiles from kinematic analysis of ref. [7] and combined strong-weak lensing measurements of ref. [8], we derive a relation between the mass profiles and the metric scalar potentials Φ and Ψ to estimate their ratio $\eta(r, z = 0.44)$ under the assumption of spherical symmetry of the cluster mass distribution. A similar analysis, that presented in ref. [9], used the mass profiles for the same cluster to obtain a constraint on the pressureless nature of dark matter. The possibility of measuring η from observations and therefore to detect deviations from the GR was discussed in ref. [10, 11], where it was pointed out that by combining constraints on the metric potentials ratio η and on the evolution of density perturbations, it is in principle possible to distinguish modifications of gravity from non-standard dark energy models. In the following, we assume a flat ΛCDM model with $\Omega_m = 0.3$ for the matter density parameter and $H_0 = 70$ km s^{-1}Mpc^{-1} for the present-day Hubble constant to convert observed angular scales into physical scales.

2 Theoretical framework

We describe the linear perturbation to the FLRW metric associated to a galaxy cluster as (e.g. ref. [12])

$$ds^2 = a^2(\tau)\left\{\left(1+2\frac{\phi}{c^2}\right)d\tau^2 - 2w_i d\tau dx^i - \left[\left(1-2\frac{\psi}{c^2}\right)\gamma(K)_{ij} + h_{ij}\right]dx^i dx^j\right\}, \qquad (2.1)$$

where w_i, h_{ij}, ϕ and ψ are functions of the coordinates that characterize the perturbation, $\gamma(K)_{ij}$ is the three-dimensional metric tensor for a space with constant curvature K. The general perturbed FLRW metric can be decomposed into scalar, vector and tensor modes, by appropriate modifications of the functions mentioned above. Since we are interested only in the scalar part of the perturbation, related to the gravitational potential, we perform a gauge transformation setting $w_i = h_{ij} = 0$. The metric in spherical coordinates takes now the form:

$$ds^2 = a^2(\tau)\left\{\left(1-2\frac{\Phi}{c^2}\right)d\tau^2 - \left(1-2\frac{\Psi}{c^2}\right)[d\chi^2 + f_K^2(\chi)d\Omega^2]\right\}. \qquad (2.2)$$

This gauge choice is called the conformal Newtonian gauge [13], for the similarity with the Newtonian limit of gravity. In the above expression Φ and Ψ are gauge-invariant scalar quantities, the Bardeen potentials (see ref. [14]), with Φ playing the role of the standard Newtonian potential. As usual, $a(\tau)$ is the expansion factor, which is a function of the conformal time τ. Finally, $f_K(\chi)$ is a function of the curvature K and the radial comoving coordinate χ, with $f_K(\chi) = \chi$ for a flat background universe with $K = 0$.

The perturbed metric of eq. 2.2 is related to the perturbation in the matter and energy content through the linearized Einstein's field equations:

$$\delta G_{\mu\nu} = \frac{8\pi G}{c^4}\delta T_{\mu\nu}.$$

If we assume the cosmological principle, the background energy momentum tensor is that of an ideal fluid,

$$T^{\mu\nu} = \left(\frac{p}{c^2} + \rho\right)u^\mu u^\nu - g^{\mu\nu}\frac{p}{c^2},$$

where ρ and p are the density and pressure of the fluid, $u^\mu = dx^\mu/d\tau$ is the four-velocity. In this case, it can be shown that the difference between the Bardeen potentials obeys the following equation in Fourier space:

$$k^2(\Psi - \Phi) = -8\pi G a^2 \bar{P}\Pi, \tag{2.3}$$

with

$$\bar{P}\Pi = \frac{3}{2}\left(\frac{k_i k_j}{k^2} - \frac{1}{3}\delta_{ij}\right)\left(T^i{}_j - \frac{1}{3}\delta_{ij}T\right)$$

the stress tensor of the fluid. Since for an ideal fluid $\bar{P}\Pi = 0$, this leads to the condition that $\Phi = \Psi$. We thus define the anisotropic stress $\eta(x)$ as the ratio $\Psi(x)/\Phi(x)$, where $x \equiv x^\mu$ are the spacetime coordinates; a deviation of this parameter from the value $\eta = 1$ indicates a violation of the Einstein's equations, i.e. a deviation from standard gravity.

In the following analysis, we carry out an observational determination of η by using the cluster mass profiles obtained from measurements of the velocity dispersion of the cluster galaxies and from combined strong and weak lensing measurements. These two methods to infer mass profiles from observational data are connected to the gravitational potentials in different ways. The motion of the galaxies in a cluster is determined by the metric time-time component only $g_{00} = -(1 + 2\Phi/c^2)$, since their typical velocities, $\sim 10^3\,\mathrm{km\,s^{-1}}$, are non-relativistic. For example, in the case of the cluster MACS 1206, the velocity dispersion along the line of sight has been measured by ref. [7] $\sigma_{LOS} = 1087^{+53}_{-55}\,\mathrm{km\,s^{-1}} \ll \mathrm{c}$. In the weak field limit the geodesic equation, for a non-relativistic particle in a gravitational field reduces to

$$\frac{d^2\vec{x}}{dt^2} = -\nabla\Phi\,.$$

Here Φ is related to the source term by the (0,0) component of the Einstein's equations, which in this context is simply given by the Poisson equation

$$\nabla^2\Phi = 4\pi G\rho\,. \tag{2.4}$$

On the other hand, photons perceive the gravitational field reflecting the contribution of both time-time and space-space metric components. This can be shown by using the general formalism of light propagation in curved spacetime. Adopting an approach similar to Faber & Visser (ref. [15]), in a spherically symmetric, static spacetime [1] (i.e. $\partial_t g_{00} = 0$ and $g_{i0} = g_{0i} = 0$) we define an effective refractive index $n(r)$ that, in the weak field approximation, is related to the perturbed metric coefficients as

$$n(r) = \left[1 - \frac{2}{c^2}\Phi_{lens} + O^{(2)}(\Phi, \Psi)\right], \tag{2.5}$$

where we set $\Phi_{lens} = (\Phi + \Psi)/2$ to be the lensing potential. Eq. 2.5 can be simply derived setting $ds^2 = 0$ in eq. 2.2 and computing $c/v \equiv n$.

Using the lensing potential, we can define a lensing density field ρ_{lens} through the Poisson equation

$$\nabla^2\Phi_{lens} = 4\pi G\rho_{lens}\,. \tag{2.6}$$

[1] In general the metric is also a function of the time coordinate, but we can safely assume that the geometry does not change during the lensing and kinematic observations.

Under the assumption of spherical symmetry one can integrate eq. 2.4 and eq. 2.6 over a sphere of radius r, thus obtaining

$$\frac{d}{dr}\Phi(r) = \frac{G}{r^2} m_{dyn}(r), \tag{2.7a}$$

$$\frac{d}{dr}\left[\Phi(r) + \Psi(r)\right] = \frac{2G}{r^2} m_{lens}(r)\,. \tag{2.7b}$$

In the above equations, $m_{dyn}(r)$ and $m_{lens}(r)$ are the total dynamic and lensing masses enclosed within a sphere of radius r. Inserting eq. 2.7a into eq. 2.7b, we derive the relation between the ratio of the Bardeen potentials and the cumulative mass profiles:

$$\eta(r) \equiv \frac{\Psi(r) - \Psi(r_0)}{\Phi(r) - \Phi(r_0)} = \frac{\int_{r_0}^{r} \frac{G}{r'^2}\left[2m_{lens}(r') - m_{dyn}(r')\right] dr'}{\int_{r_0}^{r} \frac{G}{r'^2} m_{dyn}(r') dr'}. \tag{2.8}$$

Here $\Phi(r_0)$ and $\Psi(r_0)$ are two integration constants that we can set equal to zero using the freedom in the definition of the potentials.

3 MACS 1206 and mass profiles

The galaxy cluster MACS 1206, located at redshift $z = 0.44$, is one of the 25 X-ray selected clusters observed as part of the CLASH survey.

Specifically, twenty CLASH clusters, including MACS1206, have been selected from X-ray-based compilations of dynamically relaxed systems, and the remaining five clusters have been chosen for their lensing strength [5]. MACS1206 appears as a large-scale relaxed system with a few minor overdensities in 2D distribution [16]. This result is also supported by the analysis of ref. [17], that does not find a significant level of substructures within the cluster when the most conservative selection is used to assign the membership of cluster galaxies. The concentric distribution of the mass components (stellar, gas and dark matter, see ref. [8]) further point to a relaxed status of the cluster (see also ref. [18] who demonstrate that the projected separation of the BCG and the X-ray emission peak is a robust indicator of a system's dynamical state). Moreover, the kinematic mass profile determination is in agreement with the analysis based on the *Chandra* X-ray observations under the assumption of hydrostatic equilibrium. Mass profiles based on hydrostatic equilibrium of the intra-cluster medium and on the Jeans' equation are both sensitive to the time-time component of the metric, but they feel the lack of equilibrium in different ways. Therefore, the consistent results obtained by these methods suggest that the cluster is in an equilibrium configuration (i.e. dynamically relaxed).

A first strong lensing analysis of MACS1206 was carried out in ref. [19] using 50 multiple images of 13 background lensed galaxies. An upgrade of this analysis was presented in ref. [8], exploiting a combination of strong lensing information with weak lensing shear and magnification measurements from *Subaru* multi-band images. Taking advantage of high purity sample of background galaxies derived from extensive multicolor and spectroscopic information, a robust measurement of the cluster mass density profile was obtained out to $\sim 2\,$Mpc. In the radial region between 0.3 and 0.4 Mpc, the mass profiles derived from strong lensing and weak lensing shear and magnification analyses have been shown to be consistent with each other. The resulting mass profile is parametrized according to the Navarro-Frenk-White

model (NFW hereafter), ref. [20],

$$M(r) = M_{200}\frac{\ln(1+r/r_{-2}) - (r/r_{-2})(1+r/r_{-2})^{-1}}{\ln(1+c) - c/(1+c)}, \tag{3.1}$$

where M_{200} is the mass of a sphere with overdensity 200 times the critical density of the universe at that redshift. Furthermore, r_{-2} is a scale radius that for the NFW model coincides with the radius where the logarithmic derivative of the mass density profile takes the value $d\ln\rho(r)/d\ln r = -2$. Finally, the concentration parameter c is defined as $c = r_{200}/r_{-2}$, with r_{200} the radius encompassing the mass M_{200}.

The measurement of the kinematic mass profile is presented in ref. [7] using spectroscopy information from the CLASH-VLT project (ref. [6]). Observations with VLT/VIMOS led to a total of 2749 galaxies with reliable redshift measurements in the cluster field. After the rejection of interlopers, 592 cluster members were identified. The sample was then analyzed in the projected phase-space with the *MAMPOSSt* method of ref. [21], that solves the Jeans' equation

$$\frac{d(\nu\sigma_r^2)}{dr} + 2\beta(r)\frac{\nu\sigma_r^2}{r} = -\nu(r)\frac{G\,M(r)}{r^2}\,, \tag{3.2}$$

to provide a maximum likelihood fit for the parameters of different mass models out to the virial radius ($\sim 2\,$Mpc). In eq. 3.2 $\nu(r)$ is the galaxy number density and σ_r indicates the radial velocity dispersion. The kinematic analysis also requires modeling the velocity anisotropy profile $\beta(r)$ of the tracers of the gravitational potential[2], due to the well-known mass-anisotropy degeneracy. In the original analysis of ref. [7] three models for $\beta(r)$ were considered, specifically:

$$\beta_O(r) = \beta_\infty\frac{r - r_c}{r + r_c}, \tag{3.3}$$

$$\beta_T(r) = \beta_\infty\frac{r}{r + r_c}, \tag{3.4}$$

(from ref. [22]), and constant anisotropy with no radial dependence β_C. In the above equations, β_∞ is the anisotropy value at large radii. Finally, the parameter r_c is assumed to coincide with the radius r_{-2} of the mass profile. In fact, ref. [23] proved that with this value of r_c the "O" and "T" models provide a good fit to the average anisotropy profiles predicted by a set of cosmological simulations of galaxy clusters.

The NFW model gives the highest likelihood fit to the kinematic data for the mass profiles reconstructed with the MAMPOSSt method, and in combination with the anisotropy "O" model it gives the smallest product of the relative errors in the two free parameters r_{-2} and r_{200}. In our analysis, following ref. [7], we adopt the combination of the NFW profile and the "O" model for the orbit anisotropy ("NFW+O" hereafter) as the reference model, as obtained considering the scale radius of the number density profile $r_\nu = 0.63$ Mpc. In order to estimate the dependence of the $\eta(r)$ measurement (Eq. 2.8) on the kinematic mass profile used, we also consider the Hernquist (ref. [24], hereafter "Her") and the Burkert (ref. [25], hereafter "Bur") models, that provide acceptable fits to the kinematic data (as shown in ref. [7]). In Table 1, we summarize the kinematic mass models for which we derived constraints on η.

[2]The velocity anisotropy is defined as $\beta = 1 - (\sigma_t/\sigma_r)^2$ where σ_t and σ_r are the tangential and the radial component of the velocity dispersion, respectively.

4 Results

In this section we discuss the application of eq. 2.8 to compute the anisotropic stress $\eta(r)$ for MACS 1206, using the lensing and kinematic mass profiles considered above. In our analysis, we integrated the mass profiles in the radial range $[r_0, r_{200}]$, with $r_0 = 0.55\,\mathrm{Mpc}$ and $r_{200} = 1.96\,Mpc$, where the latter is the best-fit value as obtained from both the kinematic and lensing analysis (refs. [7, 8]). At larger radii, dynamical equilibrium cannot be reliably assumed, and therefore the Jeans' equation can no longer be used to infer the gravitational potential. Moreover, at such large radii, the lensing masses become less reliable, as the weak shear signal becomes increasingly contaminated by large-scale structure filaments that might affect the recovered mass profiles.

In spite of MACS 1206 global behavior (see Section 3), in the innermost regions ($r \leq 0.5\,\mathrm{Mpc}$) we do not have sufficient information to establish whether the central core is dynamically relaxed and to confirm the validity of the spherical symmetry assumption. In fact, *Chandra* X–ray observations of MACS 1206 show an inner entropy profile (see ref. [26]) which is higher than expected for a relaxed cool core cluster, thus indicating a dynamically active core. Moreover, optical photometric observations, presented in ref. [27], show evidence for a distribution of the intracluster light (ICL) which is asymmetric with respect to the position of the BCG, with an elongation in the direction of the second brightest cluster galaxy. This suggests the presence of a tidal interaction between these two central galaxies, further questioning dynamical relaxation to hold in the central region of MACS 1206.

In our analysis we consider four parameters: r_{-2} and r_{200}, derived from the kinematic analysis in ref. [7] and r_{-2} and r_{200} derived from the lensing analysis by ref. [8]. In order to propagate the statistical errors from the mass profile parameters to $\eta(r)$, and following the analysis of ref. [9], we repeated the calculation of $\eta(r)$ by Montecarlo sampling with 10^4 trials the two probability distributions in the (r_{-2}, r_{200}) parameter space, as provided by the kinematic and by the lensing analyses. The results of these trials are shown in Figure 1 (from left to right: NFW, Hernquist and Burkert mass profiles) with red and blue points for the kinematic and lensing analysis, respectively. As discussed in ref. [9], the joint distribution of the (r_{200}, r_{-2}) parameters from the kinematic analysis has nearly zero covariance, so the errors on these two characteristic radii are almost uncorrelated. On the other hand, the joint probability distribution of the parameters from the lensing analysis can be assumed to be a bi-variate Gaussian with covariance between r_{-2} and r_{200}. As expected, the iso-probability contours in the (r_{200}, r_{-2}) plane are almost elliptical in this case (see Figure 1). In Figure 2 we plot our results for $\eta(r)$ as a function of the distance from the center, r. For our reference analysis based on the NFW+O mass model, we show the results in the range $0.55 - 1.96\,\mathrm{Mpc}$ with the red solid line, along with the corresponding 68% C.L. (orange shaded area). The effect of starting the integration of the mass profiles in eq. 2.8 from a smaller radius, namely $r_0 = 0.07$ Mpc, is shown by the black dashed curve, with the yellow area marking the corresponding 68% C.L. The errors increase when we use information from the cluster central region where the mass profile derived from strong-lensing has larger errors than the one obtained from weak-lensing (see Figure 13 of ref. [7]). Here the errors in the strong-lensing regime are dominated by model-dependent systematic uncertainties [8, 28]. The weaker constraint affects all the η profile by virtue of the correlation between errors at different radii. We also notice that the median values of $\eta(r)$ are slightly lower than those estimated when using $r_0 = 0.55$ Mpc. In both cases, the results are consistent with $\eta = 1$, thus with the predictions of GR.

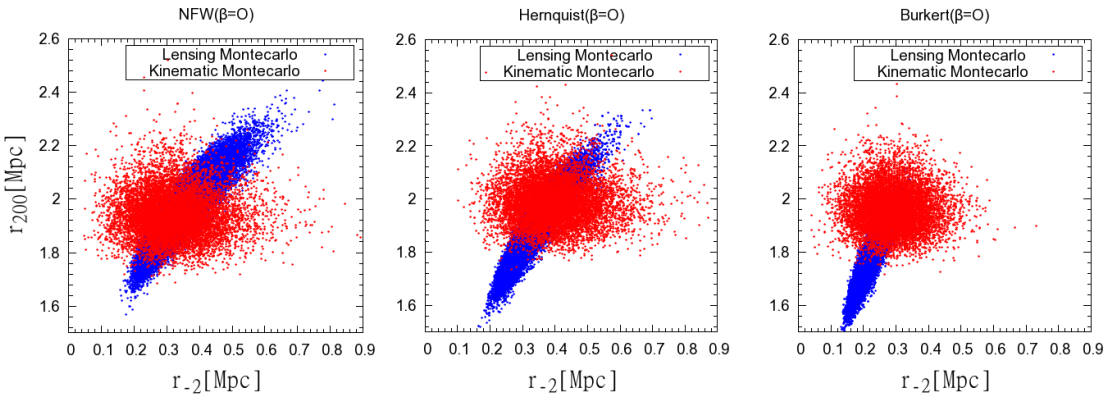

Figure 1. Results of the 10^4 Montecarlo simulations generated by sampling the joint probability distribution of r_{200} and r_{-2} from the kinematic analysis (red points) and from the combination of strong and weak lensing analyses (blue points). Left panel: NFW mass model of ref. [20]; central panel: Hernquist mass model of ref. [24]; right panel: Burkert mass model of ref. [25].

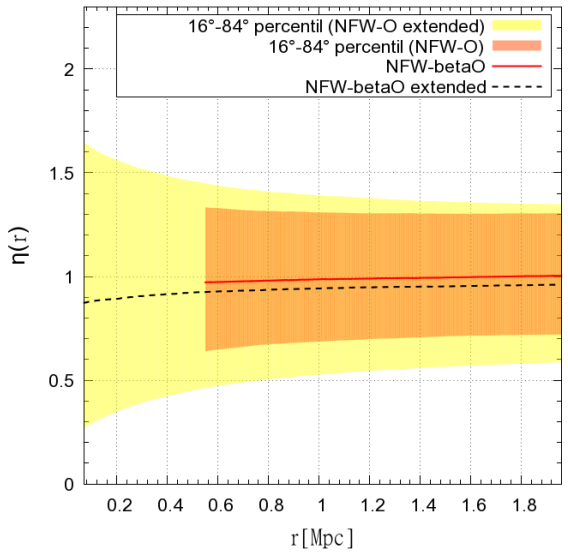

Figure 2. Constraints on the radial profile of the anisotropic stress $\eta(r)$ for the reference analysis based on the NFW parametrization of the density profile (see eq. 3.1) and the O-model of eq. 3.3 for the orbit anisotropy. Results correspond to $r_0 = 0.55$ Mpc (NFW-betaO) and 0.07 Mpc (NFW-betaO extended) for the minimum radius down to which mass density profiles are considered. Solid red and black dashed curves show the median values of $\eta(r)$, while the narrower orange and broader yellow areas mark the corresponding 68 % C.L. regions.

Possible systematic effects could in principle affect our analysis. From an observational point of view, the cluster orientation and asphericity can affect both lensing and kinematic

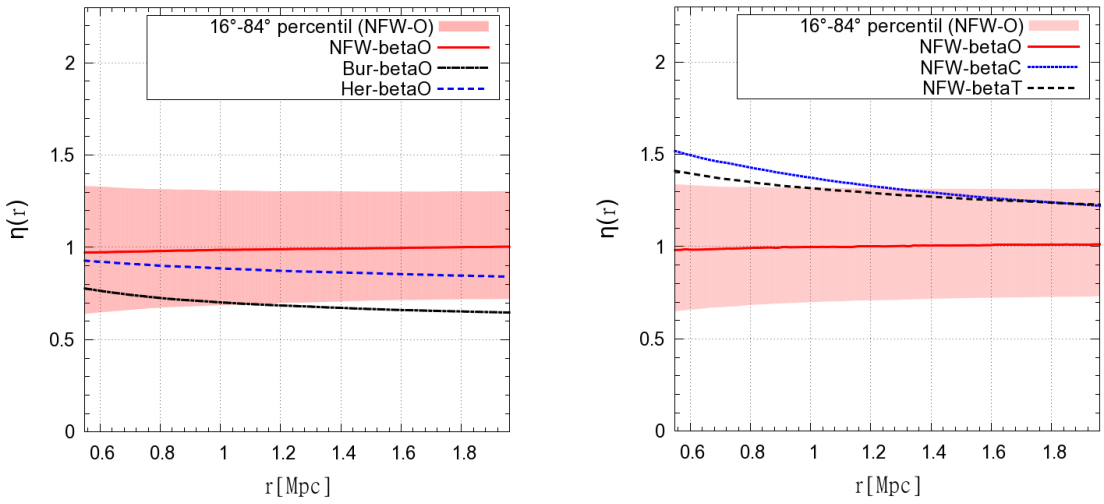

Figure 3. The effect of changing the reference model for the mass density profile (left panel) and the orbit anisotropy profile $\beta(r)$ (right panel) on the resulting constraints on the anisotropy stress profile $\eta(r)$. Here we assume $r_0 = 0.55$ Mpc. Left panel: three mass profile models with fixed anisotropy $\beta =$ "O". NFW model, ref. [20]: red solid curve; Hernquist model, ref. [24]: blue dashed curve; Burkert model, ref. [25]: black dash-dotted curve. Right panel: NFW mass profile for different anisotropy models. $\beta =$ "O": red solid curve; $\beta =$ "T": black dashed curve; $\beta =$ "C": blue dotted curve. In both panels the shaded area indicates the 68% C.L. errors for the reference NFW+O model.

mass profile determinations. Ref. [16] found that the ellipticity of the galaxy distribution for MACS1206 is $\epsilon = 0.20^{+0.05}_{-0.06}$. Such value is low especially for a medium-z cluster compared with what found at low redshift by ref. [29] ($\langle\epsilon\rangle = 0.25 \pm 0.12$ in a sample 44 Abell clusters) and by ref. [30] ($\langle\epsilon\rangle = 0.4$ for a sample of 99 Abell clusters). Moreover, since the kinematic analysis is based on the Jeans equation and thus on the assumption that the cluster is in dynamical equilibrium, the presence of substructures could affect our results on η. However, as we discuss in Section 3, MACS1206 do not show a significant level of substructures.

In Figure 3 we quantify the systematic effect on η obtained by changing all the mass and anisotropy models. We stress that all the kinematic mass and anisotropy profile combinations considered in this analysis have been proven in ref. [7] to provide acceptable fits and none of them is rejected by data. The same finding also holds for the mass profiles from the lensing analysis. In the left panel, we consider three different mass profiles (see also Table I) in both kinematic and lensing analysis, assuming in all cases $\beta =$ "O" for the orbit anisotropy. The solid, dashed and dash-dotted lines indicate the median values of the distributions for NFW, Hernquist and Burkert respectively, while the colored area indicates the 68% C.L. region for the NFW+O profile. We note that GR predictions are now slightly outside the 68% C.L. regions when using the "Bur" mass profile, thus underlining the importance of the adopted mass profile parametrization. However, we note that noting that the "Bur" model has been statistically disfavored by the ensemble mass profile derived from a stacked lensing analysis of the CLASH X-ray-selected sample, also including MACS J1206, based on strong–lensing, weak–lensing shear and magnification data [31].

In the right panel of Figure 3 we show $\eta(r)$ computed using the NFW mass profile and the three anisotropy profiles discussed in Section 3. The shaded areas indicate the 68%

Mass profile	β	η	$\Delta\eta(68\%C.L.)$	$\Delta\eta(95\%C.L.)$
NFW	O	1.00	$^{+0.31}_{-0.28}$	$^{+0.61}_{-0.54}$
NFW	C	1.22	$^{+0.45}_{-0.38}$	$^{+0.93}_{-0.68}$
NFW	T	1.23	$^{+0.33}_{-0.33}$	$^{+0.71}_{-0.61}$
Bur	O	0.65	$^{+0.26}_{-0.23}$	$^{+0.51}_{-0.44}$
Her	O	0.84	$^{+0.31}_{-0.28}$	$^{+0.66}_{-0.60}$

Table 1. Constraints on the anisotropic stress η for the different mass and anisotropy models. Column 1: mass model used (NFW: ref. [20]; Bur: ref. [25]; Her: ref. [24]). Column 2: model for the profile of orbit anisotropy as fitted in the kinematic mass reconstruction (O: eq. 3.3; T: eq. 3.4; C: constant β). Column 3: median values for η at r_{200}; Columns 4 and 5: errors at 68% and 95% C.L.

confidence regions for the reference model NFW+O while the solid, dashed and dotted lines represent the medians of the distributions. In this case, although the details of the results are sensitive to the anisotropy model adopted, the resulting η profiles always lie within the statistical uncertainties of the reference model (see also Table I).

As mentioned above, since η is obtained as a ratio of integrals depending on the mass profiles (see eq. 2.8), the errors at different radii are correlated. In fact, the determination of $\eta(r)$ at a fixed radius $\bar{r}$ is affected by the shape of the profile at $r < \bar{r}$. For this reason, we quote the values of η computed at $r_{200} = 1.96$ Mpc for all the models analyses, as reported in Table 1.

For our reference model (NFW with anisotropy profile 'O'), we obtain

$$\eta(1.96\,Mpc) = 1.00^{+0.31}_{-0.28}\,(\text{stat}) \pm 0.35\,(\text{syst}), \tag{4.1}$$

at 68 % C.L. where the systematic error is computed taking into account the variation in the median value of $\eta(r_{200})$, due to the different anisotropy and mass profiles used. As such, our analysis provides constraints on the anisotropic stress η which are fully consistent with the GR predictions. In order to highlight how these constraints compare with those derived from other cosmological probes, in the following section we will recast them in terms of constraints on the specific class of $f(R)$ modified gravity models.

5 Constraints on $f(R)$ models

Constraints on η can generally be used to set bounds on specific modified gravity models. We consider here for a moment only the statistical error given by eq. 4.1, and assume therefore that η lies between 0.7 and 1.3 at $r = 1.96$ Mpc. Then we study how this translates into constraints on one of the simplest and most investigated class of modified gravity models, namely $f(R)$ models. In this class of models, proposed first in 1970 by ref. [32] (see ref. [33] for a review), the Einstein-Hilbert Action

$$S_{EH} = \frac{1}{16\pi G}\int \sqrt{-g}Rd^4x$$

is replaced by

$$S = \frac{1}{16\pi G}\int \sqrt{-g}[R + f(R)]d^4x, \tag{5.1}$$

where $f(R)$ is a function of the curvature scalar R. Varying the action of eq. 5.1 with respect to the metric $g_{\mu\nu}$ leads to the field equations:

$$(1 + f_{,R})R_{\mu\nu} - \frac{1}{2}g_{\mu\nu}[f(R) + R] + (g_{\mu\nu}\Box - \nabla_\mu\nabla_\nu)f_{,R} = 8\pi G T_{\mu\nu}, \tag{5.2}$$

where $f_{,R} = df(R)/dR$.

The general expression for the two Newtonian potentials in $f(R)$ models in Fourier space is

$$\Phi = -\frac{4\pi G\rho_m}{1 + f_{,R}}\frac{a^2}{k^2}\left(1 + \frac{1}{3}\frac{k^2}{M^2a^2 + k^2}\right), \tag{5.3}$$

$$\Psi = -\frac{4\pi G\rho_m}{1 + f_{,R}}\frac{a^2}{k^2}\left(1 - \frac{1}{3}\frac{k^2}{M^2a^2 + k^2}\right). \tag{5.4}$$

where k is the norm of the comoving wavevector. In the above expressions for the potentials, the effective scalaron mass

$$M^2 = \frac{R}{3}\left(\frac{1 + f_{,R}}{Rf_{,RR}} - 1\right). \tag{5.5}$$

(where $f_{,RR} = d^2f(R)/dR^2$) provides the interaction range $\lambda = M^{-1}$ in the corresponding Yukawa-type potential. These expressions are valid provided there are no screening mechanisms active at the relevant scales. In standard GR $f_{,R} = 0$, $f_{,RR} = 0$ and $M \to \infty$, so that one recovers the usual expression for Ψ, Φ and for η. The expression for $\eta(r) = \Psi(r)/\Phi(r)$ is the ratio of the Fourier anti-transforms of the potentials, and one could derive directly constraints on M and $f_{,R}$ at the scale and redshift of the cluster. Since the present constraints are still dominated by systematics is probably not worth to try a very detailed comparison with theory. Therefore, our aim here is just to point out the potential of this method. In this spirit, we derive here below constraints on the parameters that characterize a $f(R)$ model.

In the limit of small scales, $k \gg M$, one has simply

$$\eta = \frac{\Psi}{\Phi} = \frac{1}{2} \tag{5.6}$$

while in the opposite limit $k \ll M$ one recovers the standard GR result $\eta = 1$. It is then clear that if we can rule out $\eta = 1/2$, which indeed appears at almost 2σ from our best fit when considering only the statistical error, we can say that the interaction scale $\lambda = M^{-1}$ should be smaller than the cluster scale, i.e.

$$\lambda < 2 \text{ Mpc}. \tag{5.7}$$

In $f(R)$ models the first derivative $f_{,R}$ is already well constrained to be much smaller than unity in order to pass cosmological constraints (see, e.g., ref. [4], and references therein); moreover, for small deviations from standard gravity $f_{,RR} \ll R^{-1}$ so we can approximate $M^2 = 1/(3f_{,RR})$ and we obtain at $z = 0.44$

$$|f_{,RR(0.44)}| < 1.3 \text{ Mpc}^2. \tag{5.8}$$

This is the first time a constraint on the second derivative of $f(R)$ is obtained without relying on a particular $f(R)$ model. However, we emphasize again that we are neglecting the systematic errors, so this constraint should be taken with some caution.

If the $f(R)$ model can be approximated near the present epoch by a power law $f(R) = \alpha R_0 (R/R_0)^{-n}$ where $R_0 \approx H_0^2$ is the present curvature scalar, then we find for the dimensionless constants α, n the constraint

$$|n(n+1)\alpha| = |(n+1)f_{,R0}| < \left(1.3H_0^2\right) \approx 10^{-7}. \tag{5.9}$$

(we are neglecting here the evolution between $z = 0.44$ and the present time). This is very close to, or better than, the current constraint $|f_{,R0}| = |\alpha n| \leq 10^{-6}$ (see e.g. refs. [34, 35]) for compatibility with background and linear perturbation theory. Of course the $f(R)$ Lagrangian can have any shape so there is no need to expect necessarily a simple connection between $f_{,R}$ and $f_{,RR}$. In general, the power of estimating η from lensing and kinematic mass profiles of clusters is that one can put an independent constraint also on the second, rather than just the first, derivative of $f(R)$ at scales of order of one Mpc, much smaller than what is obtainable from linear perturbation theory. Moreover, such constraints can be obtained independently at various redshifts and do not require a specific $f(R)$ model valid along the entire cosmic evolution which is instead needed when constraining $f(R)$ theories with the cosmic microwave background or the linear perturbation growth.

6 Conclusions

In this paper we have presented a method to derive constraints on the anisotropic stress $\eta = \Phi/\Psi$ by comparing high-precision determinations of the total mass profiles of galaxy clusters from lensing and kinematic analyses. As a case study, we have applied this method to MACS 1206, a *bona fide* relaxed cluster at $z = 0.44$ with $M_{200} = 1.4 \pm 0.2 M_\odot$ (ref.[7]). Lensing masses for MACS 1206 have been derived by ref. [8] using the high-quality imaging and photometric data obtained from HST and *Subaru* within the CLASH project. Kinematic mass profiles have been derived by ref. [7] thanks to intensive spectroscopic observations carried out within the CLASH-VLT program. Galaxy motions are sensitive only to the time-time component Φ of the metric perturbation, while lensing is sensitive to both the time-time and space-space components, i.e. to $\Phi + \Psi$. Therefore, a comparison of mass profiles based on these two independent methods allows one to set constraints on possible deviations from the prediction of General Relativity (GR), $\eta = 1$.

The results of our analysis can be summarized as follows.

- Comparing mass profiles over the range of radii from $r_0 = 0.55$ Mpc out to $r_{200} = 1.96$ Mpc, we find results to be consistent with the prediction of GR: $\eta(r_{200}) = 1.00^{+0.31}_{-0.28}$ at 68% C.L. for our reference analysis based on the NFW parametrization of the mass density profile and a specific model for the profile of orbit anisotropy.

- While the above errors refer only to statistical uncertainties, we also estimated the effects of systematic uncertainties related to changing the parametrization of the mass density and orbit anisotropy profile, as well as changing the minimum radius down to which mass profiles are considered. Within the range of models considered, these systematic uncertainties roughly double the uncertainty in the measurement of η.

- To illustrate the potential of the method, we re-phrased the constraints on η, with a 30% uncertainty, in terms of constraints on the $f(R)$ class of modified gravity models, neglecting systematics. Interestingly, we find these constraints to be competitive with those obtained by combining expansion probes, cosmic microwave background anisotropies and large-scale structure observations (e.g., refs. [4, 34, 35]). In particular, ref. [36] constrained the values of $\eta(z=0)$ and $\mu(z=0)$, where $\mu(z,k)$ represents the modification to the Poisson equation for Φ, according to

$$-k^2\Phi = 4\pi G a^2 \mu(z,k)\delta\rho, \tag{6.1}$$

  with $\delta\rho$ the overdensity of the perturbation. This analysis was based on WMAP-5 data combined with cosmic shear data from CFHTLenS and Integrated Sachs Wolf (ISW) data, taking into account also a possible time evolution of the two functions. They found $\eta(z=0) = 0.98^{+0.73}_{-1.00}$ for $z_s = 1.0$ and $\eta(z=0) = 1.30 \pm 0.35$ for $z_s = 2$, where z_s is a transition redshift at which the parameters smoothly change to their late time values, with uncertainties referring to 68% C.L.. In a similar way, ref. [37] obtained $-1.6 < \eta(0) - 1 < 2.7$ at 95% C.L. by combining CMB constraints from WMAP-5, Type-Ia SN from Union2, and cosmic shear data from CFHTLS and COSMOS surveys.

  Ref. [4] combined CMB data with different cosmological probes to study time- and scale-dependence of the modified gravity parameters η and μ, both extrapolated to $z = 0$. As a result, a tension with GR is found at $\sim 3\sigma$ C.L. when *Planck* CMB data are combined with constraints from Baryonic Acoustic Oscillations, Redshift Space Distortions and Weak Lensing data. Interestingly, the tension with ΛCDM predictions is alleviated when including in the analysis also the contribution from CMB lensing (see Table 6 and also Figures 14,17 of ref. [4]). In this case they obtain $\eta(z=0) - 1 = 0.60 \pm 0.86$ for the scale-independent determinations. They also show that the constraints become weaker when introducing the dependence on the scale.

  In general, our results are broadly consistent with the above constraints on deviations from GR, even if our method provides constraints only on η. Our statistical uncertainty in the measurement of η is quite competitive with those obtained from CMB and large-scale structure probes. However, we emphasize once again that an accurate control of the systematics in our analysis is mandatory for our proof-of-concept analysis to turn into an accurate and robust method to constrain modifications of gravity at the scales of galaxy clusters.

It is worth pointing out that the above results have been obtained from high-quality observational data of only a single galaxy cluster, thus highlighting the potential of using mass profiles of clusters as tools to probe the nature of gravity on cosmological scales. In principle, this result should not surprise; as long as the cluster in consideration satisfies the main assumptions on which lensing and kinematic mass profiles are recovered, the precision of the derived constraints is only limited by the quality of observational data. Kinematic mass profiles are based on solving the Jeans equation for the projected phase-space distribution of cluster galaxies, assuming a spherically symmetric stationary system within which galaxies moves as tracers of the underlying potential. Even though the lensing mass profile do not rely on any assumption on the dynamical state of the cluster, its reconstruction still assumes spherical symmetry, as well as negligible contamination from the surrounding large-scale structure. In this respect, the choice of MACSJ 1206 for this case study is close to be optimal, given the overall appearance of this object as dynamically relaxed system.

MACSJ 1206 is only one of a dozen clusters of the CLASH-VLT survey for which data of comparable quality are available. The extension of this analysis to other clusters requires the combination of large redshift samples, high-quality weak and strong lensing data, as well as X-ray data on well selected clusters. A sample of at least 500 redshifts of member galaxies is needed for accurate dynamical mass profiles. Together with deep X-ray data, kinematic data are also needed to check whether the system is relaxed or whether other astrophysical systematics can play a significant role. As a complementary approach, applying the same analyses to realistic cosmological simulations of galaxy clusters should quantify the impact of systematics in the measurement of lensing and kinematic mass profiles, and, ultimately, their impact in precision tests of gravity at the scale of galaxy clusters.

Acknowledgements. L.P. and S.B. acknowledge support from the PRIN-MIUR 201278X4FL grant and from the "InDark" INFN Grant. B.S., A.B. and M.G. acknowledge support from the PRIN MIUR 2010-2011 (J91J12000450001) grant and and from PRIN-INAF 2014 1.05.01.94.02. L.A. is supported by the DFG TR33 "The Dark Universe" grant. K.U. is supported by the grants MOST 103-2112-M-001-003-MY3 and MOST 103-2112-M-001-030-MY3. C.G. acknowledges support by VILLUM FONDEN Young Investigator Programme through grant no. 10123. G.B.C. is supported by the CAPES-ICRANET programme through the grant BEX 13946/13-7. This work is partially supported by "Consorzio per la Fisica di Trieste".

References

[1] Planck Collaboration, P. A. R. Ade, N. Aghanim, M. Arnaud, M. Ashdown, J. Aumont, C. Baccigalupi, A. J. Banday, R. B. Barreiro, J. G. Bartlett, and et al., *Planck 2015 results. XIII. Cosmological parameters*, *ArXiv e-prints* (Feb., 2015) [arXiv:1502.01589].

[2] A. G. Riess, A. V. Filippenko, P. Challis, A. Clocchiatti, A. Diercks, P. M. Garnavich, R. L. Gilliland, C. J. Hogan, S. Jha, R. P. Kirshner, B. Leibundgut, M. M. Phillips, D. Reiss, B. P. Schmidt, R. A. Schommer, R. C. Smith, J. Spyromilio, C. Stubbs, N. B. Suntzeff, and J. Tonry, *Observational Evidence from Supernovae for an Accelerating Universe and a Cosmological Constant*, AJ **116** (Sept., 1998) 1009–1038, [astro-ph/9805201].

[3] A. Lue, R. Scoccimarro, and G. Starkman, *Differentiating between modified gravity and dark energy*, Phys. Rev. D **69** (Feb., 2004) 044005, [astro-ph/0307034].

[4] Planck Collaboration, P. A. R. Ade, N. Aghanim, M. Arnaud, M. Ashdown, J. Aumont, C. Baccigalupi, A. J. Banday, R. B. Barreiro, N. Bartolo, and et al., *Planck 2015 results. XIV. Dark energy and modified gravity*, *ArXiv e-prints* (Feb., 2015) [arXiv:1502.01590].

[5] M. Postman, D. Coe, N. Benítez, L. Bradley, T. Broadhurst, M. Donahue, H. Ford, O. Graur, G. Graves, S. Jouvel, A. Koekemoer, D. Lemze, E. Medezinski, A. Molino, L. Moustakas, S. Ogaz, A. Riess, S. Rodney, P. Rosati, K. Umetsu, W. Zheng, A. Zitrin, M. Bartelmann, R. Bouwens, N. Czakon, S. Golwala, O. Host, L. Infante, S. Jha, Y. Jimenez-Teja, D. Kelson, O. Lahav, R. Lazkoz, D. Maoz, C. McCully, P. Melchior, M. Meneghetti, J. Merten, J. Moustakas, M. Nonino, B. Patel, E. Regös, J. Sayers, S. Seitz, and A. Van der Wel, *The Cluster Lensing and Supernova Survey with Hubble: An Overview*, ApJS **199** (Apr., 2012) 25, [arXiv:1106.3328].

[6] P. Rosati, I. Balestra, C. Grillo, A. Mercurio, M. Nonino, A. Biviano, M. Girardi, E. Vanzella, and Clash-VLT Team, *CLASH-VLT: A VIMOS Large Programme to Map the Dark Matter Mass Distribution in Galaxy Clusters and Probe Distant Lensed Galaxies*, *The Messenger* **158** (Dec., 2014) 48–53.

[7] A. Biviano, P. Rosati, I. Balestra, A. Mercurio, M. Girardi, M. Nonino, C. Grillo, M. Scodeggio, D. Lemze, D. Kelson, K. Umetsu, M. Postman, A. Zitrin, O. Czoske, S. Ettori, A. Fritz, M. Lombardi, C. Maier, E. Medezinski, S. Mei, V. Presotto, V. Strazzullo, P. Tozzi, B. Ziegler, M. Annunziatella, M. Bartelmann, N. Benitez, L. Bradley, M. Brescia, T. Broadhurst, D. Coe, R. Demarco, M. Donahue, H. Ford, R. Gobat, G. Graves, A. Koekemoer, U. Kuchner, P. Melchior, M. Meneghetti, J. Merten, L. Moustakas, E. Munari, E. Regős, B. Sartoris, S. Seitz, and W. Zheng, *CLASH-VLT: The mass, velocity-anisotropy, and pseudo-phase-space density profiles of the $z = 0.44$ galaxy cluster MACS J1206.2-0847*, A&A **558** (Oct., 2013) A1, [arXiv:1307.5867].

[8] K. Umetsu, E. Medezinski, M. Nonino, J. Merten, A. Zitrin, A. Molino, C. Grillo, M. Carrasco, M. Donahue, A. Mahdavi, D. Coe, M. Postman, A. Koekemoer, N. Czakon, J. Sayers, T. Mroczkowski, S. Golwala, P. M. Koch, K.-Y. Lin, S. M. Molnar, P. Rosati, I. Balestra, A. Mercurio, M. Scodeggio, A. Biviano, T. Anguita, L. Infante, G. Seidel, I. Sendra, S. Jouvel, O. Host, D. Lemze, T. Broadhurst, M. Meneghetti, L. Moustakas, M. Bartelmann, N. Benítez, R. Bouwens, L. Bradley, H. Ford, Y. Jiménez-Teja, D. Kelson, O. Lahav, P. Melchior, J. Moustakas, S. Ogaz, S. Seitz, and W. Zheng, *CLASH: Mass Distribution in and around MACS J1206.2-0847 from a Full Cluster Lensing Analysis*, ApJ **755** (Aug., 2012) 56, [arXiv:1204.3630].

[9] B. Sartoris, A. Biviano, P. Rosati, S. Borgani, K. Umetsu, M. Bartelmann, M. Girardi, C. Grillo, D. Lemze, A. Zitrin, I. Balestra, A. Mercurio, M. Nonino, M. Postman, N. Czakon, L. Bradley, T. Broadhurst, D. Coe, E. Medezinski, P. Melchior, M. Meneghetti, J. Merten, M. Annunziatella, N. Benitez, O. Czoske, M. Donahue, S. Ettori, H. Ford, A. Fritz, D. Kelson, A. Koekemoer, U. Kuchner, M. Lombardi, C. Maier, L. A. Moustakas, E. Munari, V. Presotto, M. Scodeggio, S. Seitz, P. Tozzi, W. Zheng, and B. Ziegler, *CLASH-VLT: Constraints on the Dark Matter Equation of State from Accurate Measurements of Galaxy Cluster Mass Profiles*, ApJ **783** (Mar., 2014) L11, [arXiv:1401.5800].

[10] L. Amendola, M. Kunz, and D. Sapone, *Measuring the dark side (with weak lensing)*, *JCAP* **0804** (2008) 013, [arXiv:0704.2421].

[11] B. Jain and P. Zhang, *Observational tests of modified gravity*, Phys. Rev. D **78** (Sept., 2008) 063503, [arXiv:0709.2375].

[12] H. Mo, F. C. van den Bosch, and S. White, *Galaxy Formation and Evolution*. May, 2010.

[13] V. Mukhanov, *Physical Foundations of Cosmology*. Mar., 2001.

[14] J. M. Bardeen, *Gauge-invariant cosmological perturbations*, Phys. Rev. D **22** (Oct., 1980) 1882–1905.

[15] T. Faber and M. Visser, *Combining rotation curves and gravitational lensing: how to measure the equation of state of dark matter in the galactic halo*, MNRAS **372** (Oct., 2006) 136–142, [astro-ph/0512213].

[16] M. Girardi, A. Mercurio, I. Balestra, M. Nonino, A. Biviano, C. Grillo, P. Rosati, M. Annunziatella, R. Demarco, A. Fritz, R. Gobat, D. Lemze, V. Presotto, M. Scodeggio, P. Tozzi, G. Bartosch Caminha, M. Brescia, D. Coe, D. Kelson, A. Koekemoer, M. Lombardi, E. Medezinski, M. Postman, B. Sartoris, K. Umetsu, A. Zitrin, W. Boschin, O. Czoske, G. De Lucia, U. Kuchner, C. Maier, M. Meneghetti, P. Monaco, A. Monna, E. Munari, S. Seitz, M. Verdugo, and B. Ziegler, *CLASH-VLT: Substructure in the galaxy cluster MACS J1206.2-0847 from kinematics of galaxy populations*, A&A **579** (July, 2015) A4, [arXiv:1503.05607].

[17] D. Lemze, M. Postman, S. Genel, H. C. Ford, I. Balestra, M. Donahue, D. Kelson, M. Nonino, A. Mercurio, A. Biviano, P. Rosati, K. Umetsu, D. Sand, A. Koekemoer, M. Meneghetti, P. Melchior, A. B. Newman, W. A. Bhatti, G. M. Voit, E. Medezinski, A. Zitrin, W. Zheng, T. Broadhurst, M. Bartelmann, N. Benitez, R. Bouwens, L. Bradley, D. Coe, G. Graves,

C. Grillo, L. Infante, Y. Jimenez-Teja, S. Jouvel, O. Lahav, D. Maoz, J. Merten, A. Molino, J. Moustakas, L. Moustakas, S. Ogaz, M. Scodeggio, and S. Seitz, *The Contribution of Halos with Different Mass Ratios to the Overall Growth of Cluster-sized Halos*, ApJ **776** (Oct., 2013) 91, [arXiv:1308.1675].

[18] D. S. Hudson, R. Mittal, T. H. Reiprich, P. E. J. Nulsen, H. Andernach, and C. L. Sarazin, *What is a cool-core cluster? a detailed analysis of the cores of the X-ray flux-limited HIFLUGCS cluster sample*, A&A **513** (Apr., 2010) A37, [arXiv:0911.0409].

[19] A. Zitrin, T. Broadhurst, R. Barkana, Y. Rephaeli, and N. Benítez, *Strong-lensing analysis of a complete sample of 12 MACS clusters at $z > 0.5$: mass models and Einstein radii*, MNRAS **410** (Jan., 2011) 1939–1956, [arXiv:1002.0521].

[20] J. F. Navarro, C. S. Frenk, and S. D. M. White, *A Universal Density Profile from Hierarchical Clustering*, ApJ **490** (Dec., 1997) 493–508, [astro-ph/9611107].

[21] G. A. Mamon, A. Biviano, and G. Boué, *MAMPOSSt: Modelling Anisotropy and Mass Profiles of Observed Spherical Systems - I. Gaussian 3D velocities*, MNRAS **429** (Mar., 2013) 3079–3098, [arXiv:1212.1455].

[22] O. Tiret, F. Combes, G. W. Angus, B. Famaey, and H. S. Zhao, *Velocity dispersion around ellipticals in MOND*, A&A **476** (Dec., 2007) L1–L4, [arXiv:0710.4070].

[23] G. A. Mamon, A. Biviano, and G. Murante, *The universal distribution of halo interlopers in projected phase space. Bias in galaxy cluster concentration and velocity anisotropy?*, A&A **520** (Sept., 2010) A30, [arXiv:1003.0033].

[24] L. Hernquist, *An analytical model for spherical galaxies and bulges*, ApJ **356** (June, 1990) 359–364.

[25] A. Burkert, *The Structure of Dark Matter Halos in Dwarf Galaxies*, ApJ **447** (July, 1995) L25, [astro-ph/9504041].

[26] K. W. Cavagnolo, M. Donahue, G. M. Voit, and M. Sun, *Intracluster Medium Entropy Profiles for a Chandra Archival Sample of Galaxy Clusters*, ApJS **182** (May, 2009) 12–32, [arXiv:0902.1802].

[27] V. Presotto, M. Girardi, M. Nonino, A. Mercurio, C. Grillo, P. Rosati, A. Biviano, M. Annunziatella, I. Balestra, W. Cui, B. Sartoris, D. Lemze, B. Ascaso, J. Moustakas, H. Ford, A. Fritz, O. Czoske, S. Ettori, U. Kuchner, M. Lombardi, C. Maier, E. Medezinski, A. Molino, M. Scodeggio, V. Strazzullo, P. Tozzi, B. Ziegler, M. Bartelmann, N. Benitez, L. Bradley, M. Brescia, T. Broadhurst, D. Coe, M. Donahue, R. Gobat, G. Graves, D. Kelson, A. Koekemoer, P. Melchior, M. Meneghetti, J. Merten, L. A. Moustakas, E. Munari, M. Postman, E. Regős, S. Seitz, K. Umetsu, W. Zheng, and A. Zitrin, *Intracluster light properties in the CLASH-VLT cluster MACS J1206.2-0847*, A&A **565** (May, 2014) A126, [arXiv:1403.4979].

[28] A. Zitrin, A. Fabris, J. Merten, P. Melchior, M. Meneghetti, A. Koekemoer, D. Coe, M. Maturi, M. Bartelmann, M. Postman, K. Umetsu, G. Seidel, I. Sendra, T. Broadhurst, I. Balestra, A. Biviano, C. Grillo, A. Mercurio, M. Nonino, P. Rosati, L. Bradley, M. Carrasco, M. Donahue, H. Ford, B. L. Frye, and J. Moustakas, *Hubble Space Telescope Combined Strong and Weak Lensing Analysis of the CLASH Sample: Mass and Magnification Models and Systematic Uncertainties*, ApJ **801** (Mar., 2015) 44, [arXiv:1411.1414].

[29] B. Binggeli, *The shape and orientation of clusters of galaxies*, A&A **107** (Mar., 1982) 338–349.

[30] P. A. M. de Theije, P. Katgert, and E. van Kampen, *The shapes of galaxy clusters*, MNRAS **273** (Mar., 1995) 30–46, [astro-ph/9409011].

[31] K. Umetsu, A. Zitrin, D. Gruen, J. Merten, M. Donahue, and M. Postman, *CLASH: Joint Analysis of Strong-Lensing, Weak-Lensing Shear and Magnification Data for 20 Galaxy Clusters*, *ArXiv e-prints* (July, 2015) [arXiv:1507.04385].

[32] H. A. Buchdahl, *Non-linear Lagrangians and cosmological theory*, MNRAS **150** (1970) 1.

[33] A. De Felice and S. Tsujikawa, *f(R) theories*, *Living Rev. Rel.* **13** (2010) 3, [arXiv:1002.4928].

[34] L. Xu, *Constraints on $f(r)$ gravity through the redshift space distortion*, *Phys. Rev. D* **91** (Mar, 2015) 063008.

[35] M. Cataneo, D. Rapetti, F. Schmidt, A. B. Mantz, S. W. Allen, D. E. Applegate, P. L. Kelly, A. von der Linden, and R. G. Morris, *New constraints on f (R) gravity from clusters of galaxies*, Phys. Rev. D **92** (Aug., 2015) 044009, [arXiv:1412.0133].

[36] G.-B. Zhao, T. Giannantonio, L. Pogosian, A. Silvestri, D. J. Bacon, K. Koyama, R. C. Nichol, and Y.-S. Song, *Probing modifications of general relativity using current cosmological observations*, Phys. Rev. D **81** (May, 2010) 103510, [arXiv:1003.0001].

[37] S. F. Daniel, E. V. Linder, T. L. Smith, R. R. Caldwell, A. Cooray, A. Leauthaud, and L. Lombriser, *Testing general relativity with current cosmological data*, Phys. Rev. D **81** (June, 2010) 123508, [arXiv:1002.1962].